Brahim Menacer[1,2], Mostefa Bouchetara[2]

NUMERICAL STUDY ON THE LUBRICATION PERFORMANCE FOR DIFFERENT COMPRESSION RING PROFILE IN DIESEL ENGINE

NUMERIČKA STUDIJA O IZVEDENOM PODMAZIVANJU KOD RAZLIČITIH PROFILA KLIPNIH PRSTENOVA U DIZEL MOTORU

Originalni naučni rad / Original scientific paper
UDK /UDC:

Rad primljen / Paper received: 2.5.2020

Adresa autora / Author's address:
[1)] Ecole Supérieure en Génie Electrique et Energétique ESGEE Oran, Algeria
email: menacer_brahim @esgee-oran.dz
[2)] Laboratory of Gas Combustion and Environment, Department of Mechanical Engineering, University of Sciences and Technology, Oran, Algeria

Keywords
- hydrodynamic lubrication
- power losses
- oil film thickness
- piston ring
- cylinder liner
- diesel engine

Ključne reči
- hidrodinamičko podmazivanje
- gubici energije
- debljina uljnog filma
- klipni prsten
- obloga cilindra
- dizel motor

Abstract

For different operating conditions of an internal combustion engine, the piston-ring-liner compartment represents one of the largest sources of friction and power losses. The present paper is a contribution to evaluate the effect of the compression ring profile on the main tribological performance of the lubricant in a four-stroke diesel engine by using the GT-suite simulation software. A one-dimensional analysis is developed for the hydrodynamic lubrication between the compression piston ring and the cylinder wall. A numerical method is applied to analyse the influence of different ring geometrical designs during the working cycle on oil film thickness, frictional force, power losses. The Takiguchi simulation model /1/ is used to validate and verify the developed numerical model. The results obtained show a relatively good qualitative and quantitative compatibility between the two applied models. The developed numerical model allows the investigation of the influence of ring design parameters to improve the tribological performance of piston engines.

Izvod

Za različite radne uslove motora sa unutrašnjim sagorevanjem, žleb za klip-prsten predstavlja jedan od najvećih izvora trenja i gubitaka energije. Ovaj rad daje doprinos u proceni uticaja profila prstena na osnovni triboloski učinak maziva u četvorotaktnom dizel motoru primenom softvera za simulaciju, GT-suite. Izvedena je jednodimenzionalna analiza hidrodinamičkog podmazivanja između kompresionog klipnog prstena i zida cilindra. Primenjena je numerička metoda za analizu uticaja različitih geometrijskih oblika prstenova u toku radnog ciklusa na debljinu filma ulja, silu trenja, gubitak energije. Takiguchi simulacioni model /1/ je upotrebljen za određivanje i proveru razvijenog numeričkog modela. Dobijeni rezultati pokazuju relativno dobru kvalitativnu i kvantitativnu kompatibilnost između dva primenjena modela. Razvijeni numerički model omogućava ispitivanje uticaja parametara konstrukcije prstena, kako bi se poboljšale triboloske performanse klipnih motora.

INTRODUCTION

The optimisation of the piston rings as important components of combustion engines can contribute to the engine friction reduction, since about 20% to 40% of the friction losses of the engine are due to the piston ring assembly. The main functions of the piston rings are the sealing between the combustion chamber and the engine crankcase, the support for the heat transfer from the piston to the cylinder wall and the control of the engine oil consumption. During the compression and working strokes, the compression ring seals the combustion gases and prevents blow-by.

Many researchers have tried to understand the mechanism of piston ring motion through numerical and experimental investigations. Radakovic et al. /2/ presented the governing equations and the appropriate numerical solution method to treat thermohydrodynamic problems implying thin-film flows in the presence of transversal compression and shear thinning. They also analysed thermal and shear effects of oil film on ring performance. Takiguchi et al. /1/ studied the variation of the oil film thickness of the top and second piston ring of a truck diesel engine during a cycle by means of clearance capacitive sensors in the sliding surfaces of the rings. For the investigation of tribological characteristics, Chaudhari et al. /3/ compared the results obtained by numerical modelling of the frictional force of the various friction sources with experimental results. Guo et al. /4/ designed three piston rings with different profiles for a diesel engine using Pro/Engineer software and analysed the stresses and displacements of the piston and piston rings. The model used was the same for each mechanism, but with different procedures and assumptions. However, they did not specify the steps in the simulation.

The objective of this work is to study the effect of three piston ring profiles on tribological parameters such as oil film thickness, ring friction, and power loss. The oil film thickness was calculated from the theoretical analysis using the GT-suite simulation software and compared with the results of Takiguchi /1/. The main aim is to identify the best ring variant that would reduce friction and contribute to improved engine performance.

MODELLING ASSUMPTIONS OF PISTON-RING-LINER

The in-cylinder pressure which is one of the inputs for the simulated engine code was modulated using the first law of thermodynamics, /5/. For the simulation model, we take into account the following assumptions /6/:

– The friction between the rings and the liner includes the lubricant shear friction given by Reynolds equation and the friction due to the Greenwood-Tripp asperity contact.
– In the piston ring modelling, we have the moments and forces for each ring. The hydrodynamic pressure distribution between running surface of the ring and the liner is determined by solving the Reynolds equation in each time step, /7/.
– The volumes are connected due to the actual clearances of ring end gaps and the actual position of the rings in the grooves. The gas flow behind the rings and between ring and groove flanks is considered.
– The oil film is taken into account between the ring running surface and liner by calculating the pressure distribution in the clearance.
– In this study, lateral pressure was neglected because only the ring-piston-liner interaction is of interest. The installed ring is in a compressed state to adapt to the cylinder, /8/.
– It is assumed that the ring contracts and extends uniformly around the circumference and that the ring sits on a single point with a running contact on the top or bottom of the groove. The contact points also seal the pressure on one side from the other, so that there is a gradual change in pressure at this contact point.
– The lubrication regime in the cylinder is influenced by the variation in piston speed, which affects the friction between the piston ring and the liner throughout the piston stroke. In this study, we consider hydrodynamic lubrication, which means that the ring always moves over a complete fluid film.
– The frictional force reaches its maximum where the piston speed is highest, i.e. the piston position is at mid-stroke. If the engine speed or oil viscosity is high, a thick oil film is formed which is not completely ejected even at dead centres where the piston speed is zero /9, 10/.
– The effect of temperature on the oil viscosity has also not been taken into account.

GOVERNING EQUATIONS FOR PISTON RING FRICTION AND LUBRICATION

Kinematic relationships of connecting rod and crank mechanism

Due to the high inertia of the connecting rod - crank system, the position of the piston will not be affected by the piston ring action. The axial position x, speed U and acceleration a of the piston relative to the liner, as a function of crankshaft angular position, measured from TDC, are given respectively by /11/:

$$x = R\cos\theta + R\sqrt{1-\left(\frac{R}{L}\right)^2\sin^2\theta}\,, \tag{1}$$

$$U = \frac{dx}{dt} = R\omega\left[\sin\theta + \frac{R}{2L}\sin 2\theta\left(1-\left(\frac{R}{L}\right)^2\sin^2\theta\right)\right], \tag{2}$$

$$a = \frac{d^2x}{dt^2} = R\omega^2\left[\cos\theta + \frac{R}{L}\frac{\cos 2\theta + \frac{R}{L}\sin^4\theta}{\left(1-\left(\frac{R}{L}\right)^2\sin^2\theta\right)^{3/2}}\right]. \tag{3}$$

where: R is the crank radius (m); L is distance between bearing centres on the connecting-rod, and the crankshaft lies in the same plane as the piston motion (m); ω is crankshaft angular velocity (1/s); and t is time (s).

Reynolds equation

In the case of hydrodynamic lubrication, the oil fully supports the load of the ring on the liner, and therefore the frictional force generated by the segment-liner interaction depends on the lubricant properties, the height and width of the film below the ring surface. To determine the frictional force, coupled equations governing the fluid mechanics of the lubricant and the forces acting on the segment have to be solved. Figure 1 shows the schematic of studied system. In the general case, the unknowns are the minimum oil film thickness c, the input wetting coordinate x_1, and the output wetting coordinate x_2. Between both coordinates, there is a transition area where the oil attaches and detaches from the ring. Although this zone has a very small axial width compared to the axial width of the ring, it has an important function in the lubrication of the system.

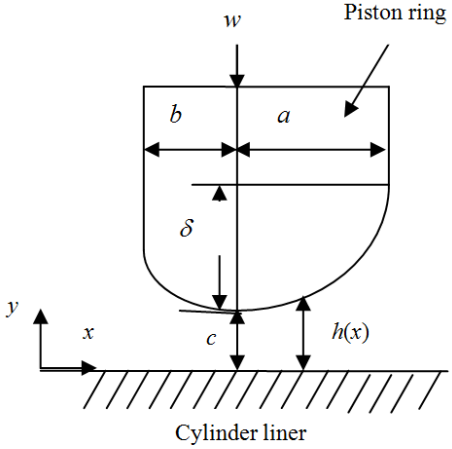

Figure 1. Hydrodynamic lubrication between ring and liner.

In Fig. 1, w is the net resultant radial force (N); a is the width of parabolic portion of the ring face (mm); b is the width of the straight portion of the ring face (mm); δ is the inclination of the wedge (°); and c is the minimal film thickness (mm).

Reynolds' equation establishes the relationship between the height, width and oil film thickness between ring and liner, and the oil pressure gradient. In the present study, a 2D approach is used in which the ring and liner lubrication parameters are determined as a function of piston position, and the Reynolds equation reduces to a 1D form. Under these conditions, the Reynolds equation is written as /12-14/:

$$\frac{\partial}{\partial x}\left(h^3\frac{\partial P}{\partial x}\right)+\frac{\partial}{\partial y}\left(h^3\frac{\partial P}{\partial y}\right)=6a\eta\frac{\partial h}{\partial x}+6v\eta\frac{\partial h}{\partial y}+12\eta\frac{dh}{dt}, \quad (4)$$

where: h is the oil film thickness under the ring as function of the coordinate distance, calculated from the leading edge of the ring x (mm); U is the piston velocity; and η lubricant viscosity (cSt).

Taking into account the symmetry of the axes along the cylinder axis, Eq.(4) becomes /15/:

$$\frac{\partial}{\partial x}\left(h^3\frac{\partial P}{\partial x}\right)=6U\eta\frac{\partial h}{\partial x}+12\eta\frac{dh}{dt}. \quad (5)$$

The variation of the film thickness under the ring with respect to position and time is, /16/:

$$h(x,t)=h_p(x)+h_r(t)+a(t)x, \quad (6)$$

where: h_p is the ring profile height (m); and h_r is the ring reference distance (m).

The surface shear stress of lubricant between two parallel plates is given by the following relationship:

$$\tau(x)=\frac{h(x)}{2}\frac{\partial P}{\partial x}-\frac{\eta U}{h(x)}. \quad (7)$$

The friction force can be obtained by integration of Eq.(7):

$$F=\int_{-b}^{a}\tau(x)dx. \quad (8)$$

The power loss is given by the following equation /9/:

$$P_u=FU=U\int_{-b}^{a}\tau(x)dx. \quad (9)$$

The Reynolds's Eq.(5) is solved by using the finite difference method and the application of the above approximations with boundary conditions. Relaxation method is used for finalizing the numerical solution, using an initial guess for film thickness Eq.(6). The Newtonian lubricant is used in the numerical scheme for the lubrication solution. The average Reynolds equation is solved to calculate the distribution of hydrodynamic pressures. The gradients of pressure depend on film thicknesses. Gauss-Seidel iterative numerical scheme is used to solve the Reynolds and the oil film thickness equations, simultaneously, and to show the maximum and minimum film thicknesses and pressure fields.

FORCES ACTING ON THE COMPRESSION RING

Contact between the ring and cylinder wall is ensured by the spring action inherent in the ring itself, which expands the ring radially, /17/. The ring can be inclined or moved axially up and down in the groove. Here, only the axial movement of the segment in the groove is taken into account and it is assumed that the surfaces of the groove are flat. The forces acting on the ring in the axial direction are shown in Fig. 2 and are expressed as follows, /18/.

The pressure force acting on the ring is given by, /19/:

$$F_p=A_r\frac{P_1-P_3}{2}, \quad (10)$$

where: A_r is the ring area in the radial direction; P_1 the pressure force in regions i = 1,2,3.

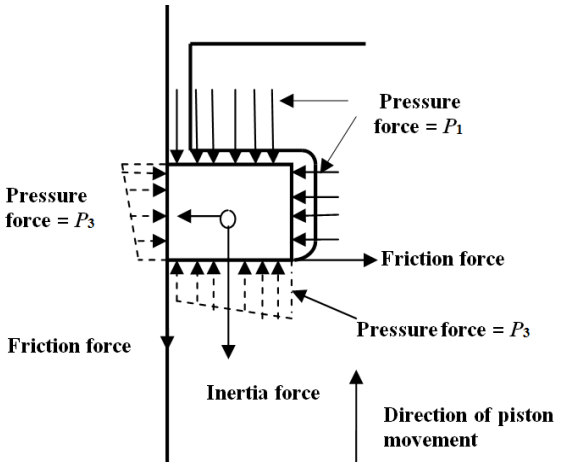

Figure 2. Forces in axial direction

The friction force is calculated from the relation, /19/:

$$F_f=fP(\pi,d_r,T_r), \quad (11)$$

with:

$$f=4.8\left(\frac{\mu U}{pT_r}\right), \quad (12)$$

where: P is the pressure behind the ring; d_r the diameter of the ring; T_r the thickness of the ring; U the piston speed in (m/s); and μ the oil viscosity in (cSt).

The inertia force is due to the mass of the ring and is calculated from the relation:

$$F_r=M_r a, \quad (13)$$

where: M_r is ring mass (kg); a is piston acceleration (m/s^2).

ADDITIONAL MODELLING CONSIDERATIONS

To solve the Reynolds equation, the boundary conditions $P(x = –b) = P_1(t)$, $P(x = a) = P_2(t)$, and the piston position during the engine operating cycle must be taken into account, Fig. 3. The vertical velocity of the body $V_B = dc/dt$ is determined by the balance between the liner of the ring force W and the lifting force due to lubricant pressure, expressed by, /18/:

$$W=\int_{-b}^{a}P(x,t)dx. \quad (14)$$

The compression ring profile plays an important role in the entertainment of the lubricant between the top piston and cylinder liner. Figure 4 and Table 1 show the different top ring profiles and its properties used in this study. The cylindrical shape of the ring provides better hydrodynamic lubrication conditions and the axially shorter contact surface to the liner surface improves sealing. In addition, the negative effects of cylinder deformations during engine operation can be better compensated. Piston rings of this profile type are actually used as compression rings.

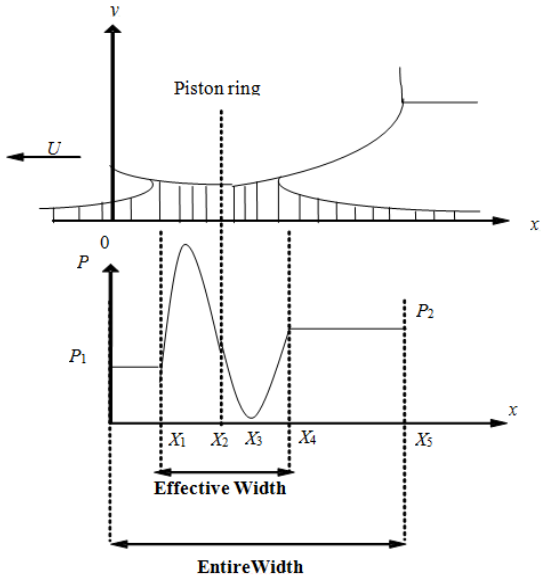

Figure 3. Open-end boundary conditions.

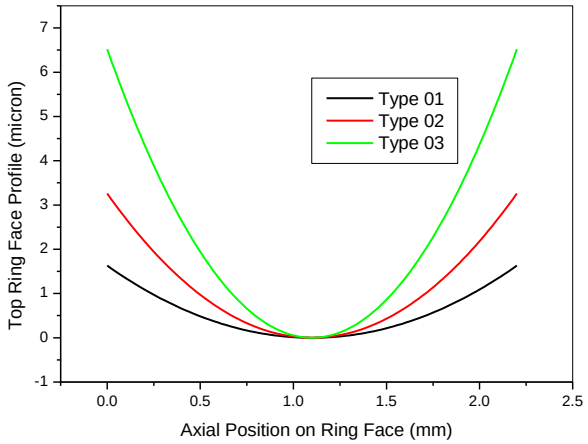

Figure 4. Investigated compression ring profiles.

Table 1. Compression ring profile property.

Property	Type I	Type II	Type III
ring surface upper profile height	1.5 μm	3.5 μm	6.5 μm
ring surface lower profile height	1.5 μm	3.5 μm	6.5 μm
ring surface crest position	5 mm	5 mm	5 mm

RESULTS AND DISCUSSION

Table 2 presents data used in this investigation. The determination of tribological performance is carried out under full load of a diesel engine and at engine speed of 2000 rpm.

Table 2. Engine data.

Parameter	Value	Units
connecting rod length	127	mm
crank radius	31.5	mm
ring axial width	1.63	mm
ring radial width	2.63	mm
bore radius	48	mm
ring density	7900	kg/m^3
ring elastic pressure	93539	N/m^2
ring modulus of elasticity	2.05 e11	Pa
engine speed	2000	rpm
oil density	881.5	kg/m^3
oil viscosity	0.008736	Pa-s

The piston speed can be determined by deriving the equation that calculates the distance between the piston and top dead centre. Figure 5 shows the variation of piston position and speed as a function of crankshaft angle at 2000 rpm for a diesel engine. Piston ring lift is due to piston acceleration, which is the derivative of piston speed equation, Fig. 6.

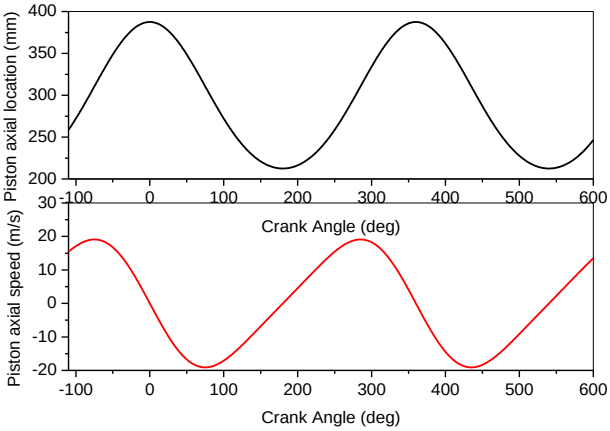

Figure 5. Piston position and speed versus crank angle.

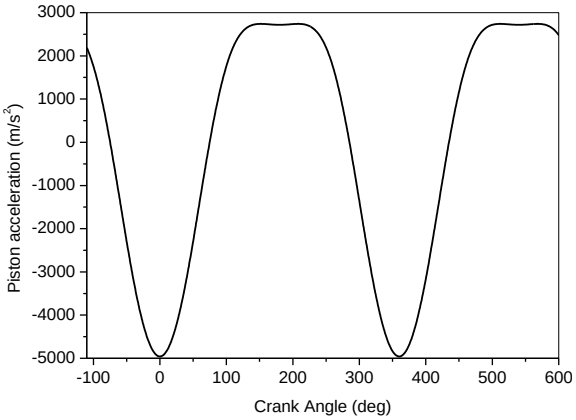

Figure 6. Piston acceleration versus crank angle at 2000 rpm.

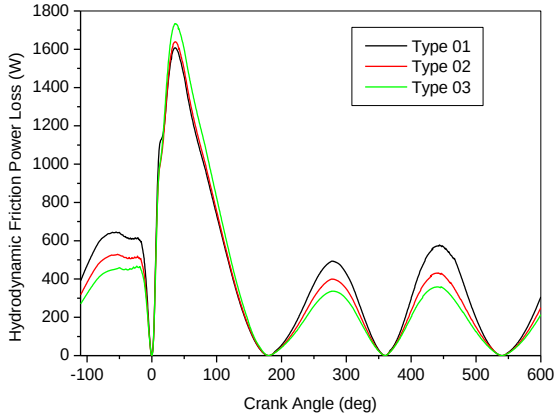

Figure 7. Effect of compression ring profile on hydrodynamic power losses versus crank angle.

Figure 7 shows the variation of hydrodynamic power losses versus crank angle for different compression ring profile at full load and at 2000 rpm engine speed. During the operating cycle of the engine, the maximum power losses for all three ring variants are all reached at mid-stroke of the piston and then cancel each other out at TDC and BDC,

corresponding to the piston velocity variation, Fig. 5. The oil film thickness and the hydrodynamic shear increase also at mid-stroke.

Figure 8 presents the variation in asperity friction power loss during a full load engine cycle at 2000 rpm. The maximum values are in the expansion phase and minimum values in the other phases of the engine cycle. It can be attributed to the fact that there is an increase in asperity contact near the TDC and BDC due to the mixed lubrication regime, whereas hydrodynamic lubrication exists for most part of the stroke. The type 03 of ring design presents higher values.

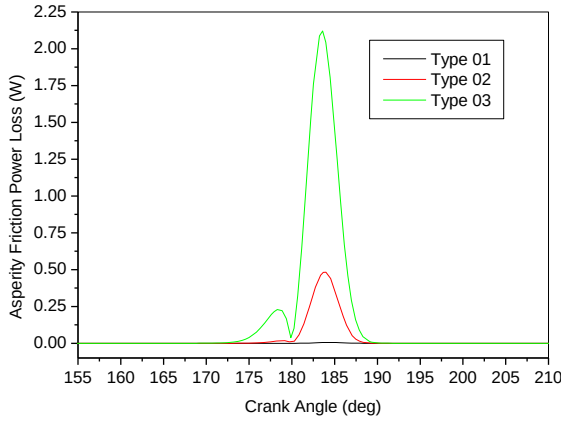

Figure 8. Variation in asperity friction power loss during a full load engine cycle at 2000 rpm.

Figure 9 shows the variation of hydrodynamic friction force versus crank angle for different ring profiles. This maximum friction value is at point of maximum cylinder pressure. The negative part of the curve is due to the change of piston speed direction through the reciprocating motion. It has been observed that the highest friction force value occurred during the expansion stroke (from –110° to 180°) with a peak of 235 N just after TDC firing. The friction was found maximum for type 1 ring profile, on the other hand type 3 has minimum friction force. At TDC, the film thickness for type 3 profile is found to be lowest. It is expected that the friction due to lubricant viscosity is minimum.

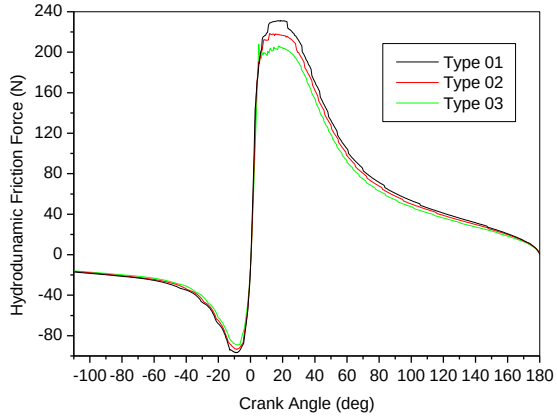

Figure 9. Hydrodynamic friction force for different ring profiles at 2000 rpm.

In general, the maximum asperity frictional force is reached at TDC and BDC during the operating cycle, due to the low critical speed and, consequently, the low oil flow at these points. Figure 10 shows the asperity frictional force between the upper ring and the cylinder liner as a function of the crankshaft angle for different ring profiles at an engine speed of 2500 rpm and full load. Type 1 has the lowest asperity friction force, followed by type 2, and the highest force with type 3, especially at TDC after the compression stroke.

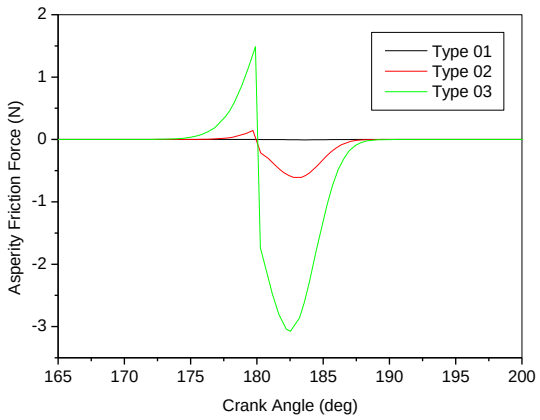

Figure 10. Effect of top ring profile on asperity friction forces at 2000 rpm.

Figure 11 shows the variation of maximum contact oil pressure as a function of the crank angle for different ring profiles. The maximum value of the hydrodynamic oil pressure is reached near the TDC. Ring profile type 3 has the maximum oil pressure, followed by type 2 and type 3, with minimum oil pressure.

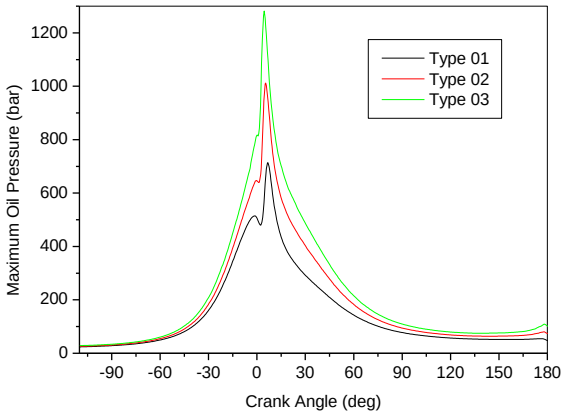

Figure 11. Effect of top ring profile on the maximum oil pressure versus crank angle for near TDC at 2000 rpm.

Figure 12 shows the variation in film thickness for different types of ring profile. The Takiguchi model /1/ was used to validate the results obtained by the developed model. The film thickness is maximum at mid-point of the different cycle phases. In the expansion stroke, the oil film thickness is lower. At the dead centres, the film is very thin, especially at the BDC after the expansion stroke and at the TDC at the beginning of the intake stroke, which can lead to high wear of the cylinder wall, due to contact between the surfaces. It can be observed that type 1 of the ring face profile provides a thicker film than the other two variants.

Figure 13 shows the variation in shear rate as a function of crank angle for different compression ring profiles. The

maximum shear rates vary over the cycle from 1.5×10^{-6} to 3.0×10^{-6} s^{-1}. Type 1 has a higher effective oil film shear rate, followed by type 2 and the lowest with type 3.

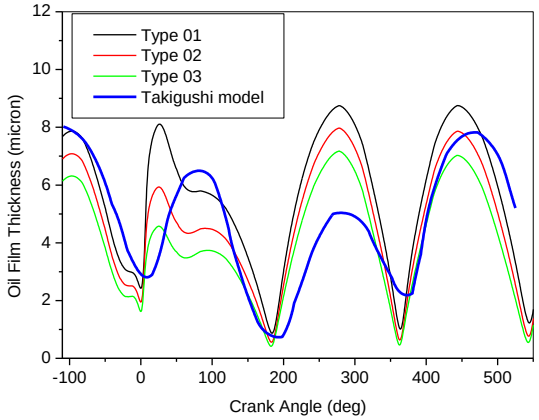

Figure 12. Minimum oil film thickness for different ring profiles during engine cycle for 2000 rpm and Takiguchi model, /1/.

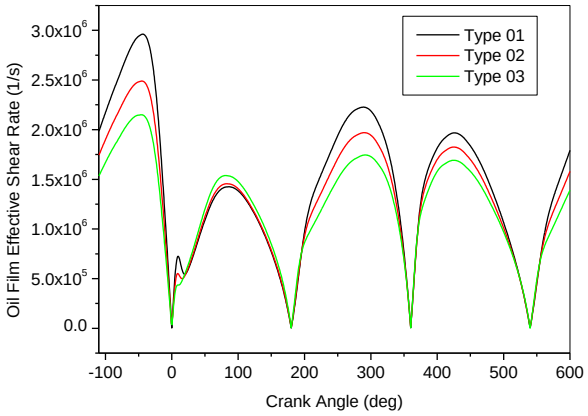

Figure 13. Oil film effective shear rate for different ring profiles during engine cycle.

Figure 14 shows the variation of friction tension as a function of crank angle for different compression ring profiles. In the combustion and expansion period, there is a noticeable change in the frictional tension. The variant of type 1 has higher frictional tensions than the other variants.

Figure 15 illustrates the gap variation versus the crank angle for different ring profiles. A remarkable change in the gap is observed in the combustion and expansion period.

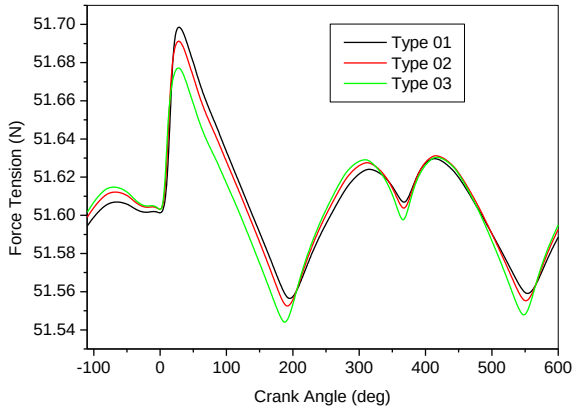

Figure 14. Friction tension with respect of crank angle for different compression ring profile.

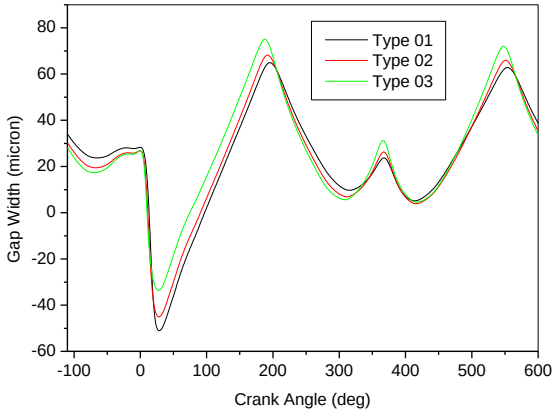

Figure 15. Gap width with versus crank angle for different ring profile.

CONCLUSION

The theoretical results obtained with the numerical model developed prove that the profile of the compression rings has an important effect on the tribological behaviour of the system piston ring-cylinder liner. The modification of the compression ring profile contributes to the reduction of frictional power losses and thus to the improvement of the tribological performance of the internal combustion engine. The increase in asperity contact causing low oil films at TDC and BDC as well as friction asperity power losses can be observed. At mid-stroke of the piston motion, thicker oil films are observed despite the presence of higher hydrodynamic frictional forces and lower oil viscosity. There is a good agreement between the results obtained with the developed numerical model and those of the Takiguchi model. In the present study, the following results could be deduced:

- The lowest frictional force is for the type 3 ring profile, which results in a reduction in engine friction losses and an increase in lubricant and fuel economy.
- The minimum oil film thickness for type 3 compression ring profile does not necessarily mean a higher frictional force and shear stress. Despite a minimum oil film thickness, the wear rate is not affected.

In future work, it would be advisable to take the blow-by phenomenon into account and analyse its effect on the ring motion in the piston groove and on the tribological behaviour of the piston-ring-cylinder liner assembly.

REFERENCES

1. Harigaya, Y., Suzuki, M., Takiguchi, M. (2003), *Analysis of oil film thickness on a piston ring of diesel engine: Effect of oil film temperature*, J Eng. Gas Turbines Power, 125(2): 596-603. doi: 10.1115/1.1501078
2. Radakovic, D.J., Khonsari, M.M. (1997), *Heat transfer in a thin-film flow in the presence of squeeze and shear thinning; Application to piston rings*, ASME J Heat Transfer, 119(2): 249-257. doi: 10.1115/1.2824217
3. Chaudhari, T., Sutaria, B. (2016), *Investigation of friction characteristics in segmented piston ring liner assembly of IC engine*, Perspect. Sci. 8: 599-602. doi: 10.1016/j.pisc.2016.06.032
4. Guo, Y.B., et al. (2011), *Analysis of piston ring lubrication with different lubricant supply*, Adv. Mater. Res. 199-200: 700-706. doi: 10.4028/www.scientific.net/AMR.199-200.700
5. Sonthalia, A., Kumar, C.R. (2013), *The effect of compression ring profile on the friction force in an internal combustion engine*, Tribol. Industry, 35(1): 74-83.

6. Soualmia, A., Bouchetara, M. (2015), *Numerical modelling of the hydrodynamic behaviour of the couple piston liner*, Mechanika, 21(6): 450-456. doi: 10.5755/j01.mech.21.6.7035
7. Arcoumanis, C., Duszynski, M., Flora, H., Ostovar, P. (1995), *Development of a piston-ring lubrication test-rig and investigation of boundary conditions for modelling lubricant film properties*, SAE Trans. 104(4): 1433-1451. https://www.jstor.org/stable/44615179
8. Wakuri, Y., et al. (1995), *Studies on friction characteristics of reciprocating engines*, Paper presented at 'Fuels and Lubricants Meeting and Exposition,' Toronto, ON, Canada, 1995. doi: 10.4271/952471
9. Jeng, Y.-R. (1992), *Theoretical analysis of piston-ring lubrication, Part I-fully flooded lubrication*, Tribol. Trans. 35(4): 696-706. doi: 10.1080/10402009208982174
10. Wannatong, K., Chanchaona, S., Sanitjai, S. (2008), *Simulation algorithm for piston ring dynamics*, Simul. Model. Pract. Theory, 16(1): 127-146. doi: 10.1016/j.simpat.2007.11.004
11. Usman, A., Park, C.W. (2016), *Optimizing the tribological performance of textured piston ring-liner contact for reduced frictional losses in SI engine: Warm operating conditions*, Tribol. Int. 99: 224-236. doi: 10.1016/j.triboint.2016.03.030
12. Delprete, C., Razavykia, A. (2018), *Piston ring-liner lubrication and tribological performance evaluation: A review*, Proc, of the Instit. of Mech. Eng., J Eng. Tribol. 232(2): 193-209. doi: 10.1177/1350650117706269
13. Delprete, C., Razavykia, A., Baldissera, P. (2020), *Detailed analysis of piston secondary motion and tribological performance*, Int. J Engine Res. 21(9): 1647-1661. doi: 10.1177/1468087419833883
14. Notay, R.S., Priest, M., Fox, M.F. (2019), *The influence of lubricant degradation on measured piston ring film thickness in a fired gasoline reciprocating engine*, Tribol. Int. 129: 112-123. doi: 10.1016/j.triboint.2018.07.002
15. Balakrishnan, S., Rahnejat, H. (2005), *Isothermal transient analysis of piston skirt-to-cylinder wall contacts under combined axial, lateral and tilting motion*, J Appl. Phys. D, Appl. Phys. 38(5): 787-799. doi: 10.1088/0022-3727/38/5/018
16. Morris, N., et al. (2013), *The influence of piston ring geometry and topography on friction*, Proc. Instit. Mech. Eng., Part J: J Eng. Tribol. 227(2): 141-153. doi: 10.1177/1350650112463534
17. Zavos, A.B., Nikolakopoulos, P.G. (2015), *Simulation of piston ring tribology with surface texturing for internal combustion engines*, Lubric. Sci. 27(3): 151-176. doi: 10.1002/ls.1261
18. Mohamad, S.A., Lu, X., Zheng, Q. (2015), *Numerical modeling of lubrication of piston ring of two-stroke marine diesel engine considering the effect of multi-scale grooves on the cylinder liner*, Proc. Instit. Mech. Eng., Part J: J Eng. Tribol. 229(8): 989-1002. doi: 10.1177/1350650114556400
19. Bertocchi, L., et al. (2013), *Fluid film lubrication in the presence of cavitation: a mass-conserving two-dimensional formulation for compressible, piezoviscous and non-Newtonian fluids*, Tribol. Int. 67: 61-71. doi: 10.1016/j.triboint.2013.05.018